Mon. Not. R. Astron. Soc. **321**, 254–268 (2001)

The template type Ia supernova 1996X

M. E. Salvo,[1★] E. Cappellaro,[1] P. A. Mazzali,[2,3] S. Benetti,[4] I. J. Danziger,[2] F. Patat[5] and M. Turatto[1]

[1]*Osservatorio Astronomico di Padova, Vicolo dell' Osservatorio 5, I-35122 Padova, Italy*
[2]*Osservatorio Astronomico di Trieste, Via Tiepolo 11, I-34131 Trieste, Italy*
[3]*Research Centre for the Early Universe, School of Science, University of Tokyo, Bunkyo-ku, Tokyo 113-0033, Japan*
[4]*Telescopio Nazionale 'Galileo', Apartado de Correos 565, E-38700 Santa Cruz de La Palma, Canary Islands, Spain*
[5]*European Southern Observatory, Karl-Schwarzschild Straße 2, D-85748 Garching bei München, Germany*

Accepted 2000 August 28. Received 2000 June 30; in original form 2000 March 29

ABSTRACT

UBVRIJ photometry and optical spectra of the type Ia SN 1996X obtained at the European Southern Observatory (ESO) during a 1-yr-long observational campaign are presented, and supplemented by late-time *Hubble Space Telescope (HST)* photometry. Spectroscopically, SN 1996X appears to be a 'normal' SN Ia. The apparent magnitude at maximum was $B = 13.24 \pm 0.02$, and the colour $B - V = 0.00 \pm 0.03$. The luminosity decline rate, $\Delta m_B(15) = 1.31 \pm 0.08$, is close to average for a SN Ia. The best estimate of the galactic extinction is $A_B = 0.30 \pm 0.05$, and there is evidence that reddening within the parent galaxy is negligible.

Detailed comparison of the light and colour curves of various 'normal' SNe Ia shows that the assumption that multicolour light curves can be described simply as a one-parameter family is not perfect. Together with problems in the calibration of the templates, this may explain the discrepancies in the distance modulus derived adopting different calibrations of the absolute magnitude versus light-curve shape relations. Indeed, we found that M_B ranges from -19.08 to -19.48 and μ ranges from 32.02 to 32.48 depending on the method used.

Computations of model light-curve and synthetic spectra for both early and late times confirm that 1996X is a normal type Ia SN and that a satisfactory fit can be obtained using a W7 progenitor structure only if we adopt the short distance. A larger distance would imply too large a Ni mass for this fainter than average SN Ia.

Key words: supernovae: general – supernovae: individual: SN 1996X – galaxies: individual: NGC 5061.

1 INTRODUCTION

One of the most exciting and unexpected results in recent astronomy is the apparent necessity for a finite cosmological constant, the result of measuring cosmic distances using type Ia Supernovae (SNe Ia) as distance indicators. This result relies heavily on the assumption that the absolute magnitude of SNe Ia can be calibrated accurately based on the observed luminosity evolution (Riess et al. 1998a; Perlmutter et al. 1999).

The suggestion that the absolute magnitude of SNe Ia correlates with the luminosity decline rates dates back to Pskovskii (1967, 1977). However, only in the last decade, with the improvement in photometric accuracy made possible by charge-coupled device (CCD) detectors, has this correlation been quantified, although its calibration and range of application are still debated (Phillips 1993; Hamuy et al. 1996a–c; Riess et al. 1996, 1998a; Phillips et al. 1999). Nearby SNe are essential for this approach because their absolute luminosity can be calibrated accurately using other distance indicators, e.g. Cepheid variables (Sandage et al. 1996; Madore et al. 1999) or the globular cluster luminosity function (GCLF) (Della Valle et al. 1998; Drenkhahn & Richtler 1999).

Theoretically, the effort to build a scenario consistently linking progenitor and explosion to explain the observed diversity of SNe Ia is still in the very early stages (Höflich, Wheeler & Thielmann 1998; Umeda et al. 1999). At this stage, high signal-to-noise observations of the spectroscopic and photometric evolution of nearby SNe Ia can provide valuable information. Unfortunately, good photometric coverage around maximum light and sufficient monitoring of the decline phase is available only for very few nearby SNe Ia, and thus it is very important to enlarge the sample. SN 1996X is one such object.

SN 1996X, was discovered independently by Evans and

★ E-mail: salvo@pd.astro.it

Takamizawa on April 12.5 UT (IAU Circ. No 6380). The SN was located at RA = $13^h18^m01^s.13$, Dec. = $-26°50'45''.3$ (equinox 2000.0), that is 52 arcsecW and 31 arcsecS of the nucleus of the elliptical galaxy NGC 5061 (Fig. 1). Early spectroscopic observations at different sites (cf. IAU Circ. No 6381) showed that SN 1996X was a type Ia SN caught before maximum light, which motivated an extensive observational campaign with the European Southern Observatory (ESO) telescopes.

SN 1996X was also observed at other observatories, in particular at CTIO (Riess et al. 1999) (http://www.ctio.noao.edu/~riccov/sn96x.gif) and at Mt Whipple. A near-infrared spectrum was published by Bowers et al. (1997).

Interestingly, Wang, Wheeler & Höflich (1997) claimed that SN 1996X showed evidence of intrinsic polarization, suggesting an asphericity of ~10 per cent in the elements distribution in the region of partial burning. This is the first time polarization was measured in a SN Ia.

Finally, the SN field was observed at two late epochs with the WFPC2 on board the *Hubble Space Telescope (HST)* (*HST* Data Archive).

In this paper we present the ESO observations, summarized in the *UBVRIJ* light curves and in the description of the evolution of the optical spectra. In addition, we discuss some spectral modelling, and compare SN 1996X with other SNe Ia within the framework of using SNe Ia as distance indicators.

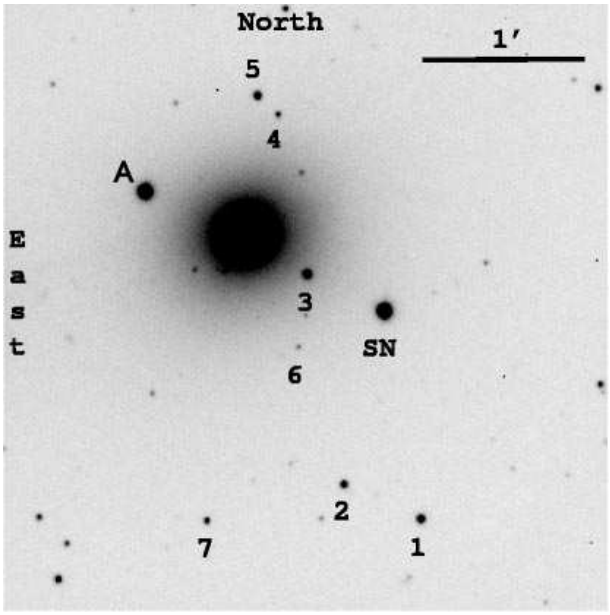

Figure 1. Identification chart for SN 1996X and for the stars of the local sequence (*V*-band exposure obtained on 1996, April 15th, with the Dutch 0.9-m telescope).

2 OBSERVATIONS AND DATA REDUCTION

2.1 Photometry

Photometry of SN 1996X was obtained mainly using the Dutch 0.9-m telescope at ESO, La Silla (CCD TK33; scale 0.44 arcsec pixel^{-1}). In addition, we used the ESO/MPI 2.2-m telescope with EFOSC2 (CCDs TK19, 0.33 arcsec pixel^{-1}; Loral 40, 0.26 arcsec pixel^{-1}), the ESO 3.6-m telescope with EFOSC1 (CCD TK26; 0.34 arcsec pixel^{-1}) and the ESO 1-m DENIS telescope (CCD TK, 0.7 arcsec pixel^{-1}). Other observations were obtained at Asiago with the 1.82-m telescope (CCD TK512M; 0.34 arcsec pixel^{-1}).

The frames were reduced using standard IRAF packages. Photometric nights were calibrated with observations of Landolt (1992) standard stars and used to define a local standard sequence which, in turn, was used to calibrate frames obtained under non-photometric conditions. The stars of the local sequence are identified in Fig. 1 and their magnitudes are listed in Table 1 along with rms deviations of the measurements obtained on different nights.

Infrared photometry was obtained at the ESO/MPI 2.2-m telescope, equipped with IRAC2 (detector NICMOS-3+lens LB, scale 0.278 arcsec pixel^{-1}), and at the ESO 1-m DENIS telescope (NICMOS-3, 2.81 arcsec pixel^{-1}).

Calibration of the infrared photometry was performed as described in Lidman, Gredel & Moneti (1997). As a check for photometric conditions we monitored star A (identified in Fig. 1), which was measured at $J = 10.53 \pm 0.01$.

The SN was located in a region of smoothly varying background, and thus reliable estimates of the SN magnitude could, in principle, be obtained with plain aperture photometry. However, we preferred to use a point spread function (PSF) fitting technique (Turatto et al. 1993), because: (i) the number of stars in the field was sufficient to measure the PSF and (ii) this method is less sensitive than aperture photometry to contamination by bad pixels and cosmic rays.

Observations of SN 1996X at late phases were obtained with the WFPC2 on board *HST* on two epochs: 1997, April 5 (F555W and F814W filters) and 1997, September 1 (F439W, F450W, F555W and F606W filters). The calibrated exposures were retrieved from the ST-ECF HST archive, properly aligned and combined to eliminate cosmic rays. At the two epochs pointing and camera orientation were quite different and the field overlap is only a small area around the SN. The instrumental magnitudes of the SN and of a foreground star (#8 in Fig. 2) were converted to the Landolt *UBVRI* system following the prescription of Holtzman et al. (1995). The April 5 observations are bracketed by ground based observations, so that it was possible to verify that, within the

Table 1. Magnitudes for the stars of the local sequence in the field of SN 1996X. The stars are identified in Figs 1 and 2.

id	*U*	*B*	*V*	*R*	*I*
1	17.99 ± 0.02	17.26 ± 0.01	16.34 ± 0.01	15.78 ± 0.02	15.25 ± 0.01
2	18.35 ± 0.03	17.76 ± 0.01	16.90 ± 0.02	16.43 ± 0.01	15.97 ± 0.01
3	17.27 ± 0.02	16.82 ± 0.01	15.90 ± 0.01	15.38 ± 0.01	14.89 ± 0.01
4	18.89 ± 0.03	18.74 ± 0.01	17.94 ± 0.01	17.49 ± 0.01	17.08 ± 0.01
5	17.15 ± 0.02	17.16 ± 0.01	16.48 ± 0.02	16.04 ± 0.01	15.66 ± 0.03
6	19.52 ± 0.01	19.62 ± 0.02	19.02 ± 0.01	18.70 ± 0.02	18.26 ± 0.02
7	19.03 ± 0.03	18.51 ± 0.02	17.67 ± 0.01	17.16 ± 0.01	16.67 ± 0.01
8		23.44 ± 0.04	22.52 ± 0.04		21.24 ± 0.04

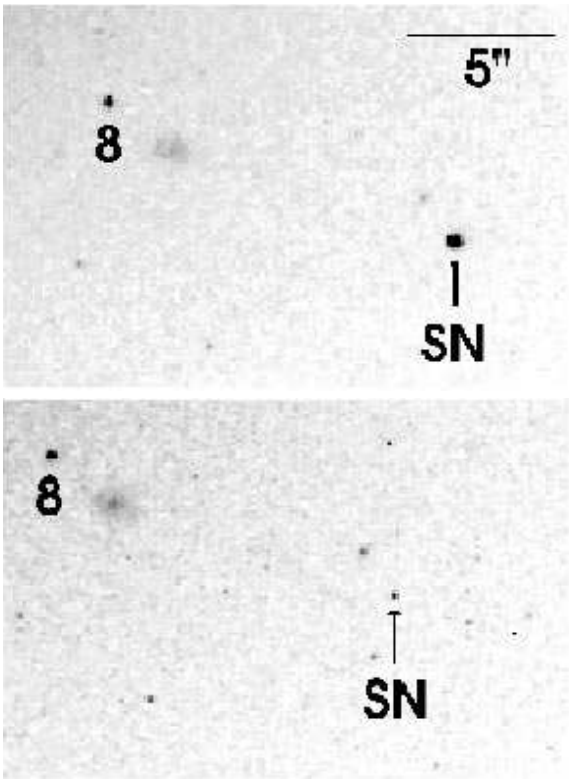

Figure 2. WFPC2 observations of SN 1996X on 1997; April 5 (top panel) and September 1 (bottom panel).

errors, the converted *HST* and ground-based photometry are consistent.

The SN optical magnitude is reported in Table 2, and the infrared (IR) ones in Table 3. The error estimates include the uncertainties in the internal calibration of the local sequence and in the PSF fitting. The latter dominates at late phases when the SN becomes faint.

An external check on the reliability of the SN photometry can be obtained by comparing our results with those recently published by Riess et al. (1999).

This is done in Fig. 3, where we plot for the various photometric bands the difference between our estimates of the SN 1996X magnitudes and those of Riess et al. These have been interpolated to the epochs of our observations using cubic splines, but only if the phase difference was less than 3 d. Error bars were obtained by adding in quadrature the errors on the individual points as reported for each source.

Although it is comforting that systematic differences are small (in all bands $\langle \Delta m \rangle \leq 0.05$), the deviations of single points are larger than expected from the combined errors. A similar conclusion was reached by Jha et al. (1999) when comparing their own photometry of SN 1998bu with that of Suntzeff et al. (1999). They attributed this problem to differences in the filters used at different observatories (which are enhanced by the peculiar and fast evolving SN spectra) and to the difficulty in measuring the SN itself (see also Suntzeff 2000). Indeed, the deviations appear to be more pronounced in the *I*-band, which is difficult to define and maintain properly because CCDs do not provide a fixed red-wavelength cutoff. The same is true for the *U*-band at the other end of the optical spectrum but, since Riess et al. did not publish *U* photometry for SN 1996X, a similar test could not be performed.

Therefore, one should be wary of overinterpreting small differences in the light curves of SNe Ia obtained with different instruments, especially for the *U* and *I*-bands.

2.2 Spectroscopy

Most of the spectroscopic observations were obtained with the ESO 1.5-m telescope equipped with a Boller & Chivens spectrograph. Other observations were obtained using the ESO/MPI 2.2-m+EFOSC2 and the ESO 3.6-m+EFOSC1. One spectrum was obtained at Asiago with the 1.82-m telescope and a B&C spectrograph.

The journal of the spectroscopic observations is given in Table 4. The overall spectral evolution is shown in Fig. 9. Two of the spectra displayed are the result of merging spectra obtained using different grisms during the same night.

Spectra were reduced using standard IRAF routines. He–Ar lamp exposures were used for wavelength calibration, and observations of spectrophotometric standard stars (Hamuy et al. 1992, 1994) for flux calibration. The absolute flux calibration of the spectra was checked against the photometry and the flux scale was adjusted if necessary.

3 INTERSTELLAR ABSORPTION

SN 1996X exploded in the outskirts of an early-type galaxy, and therefore extinction in the parent galaxy should be negligible. Indeed, our higher-resolution spectra show no evidence of interstellar absorption lines at the host galaxy rest frame.

However, a faint narrow Na I D absorption (equivalent width, EW = 0.27 Å) is detected at the rest wavelength. This can be attributed to interstellar gas in our own Galaxy. Indeed, Munari & Zwitter (1997), studying a sample of galactic early-type stars, have shown that there is a tight correlation between EW(Na I D) and interstellar reddening. Using their calibration we obtain for SN 1996X, $E(B-V) = 0.10 \pm 0.03$ mag, while a similar relation obtained by Barbon et al. (1990) for SNe Ia gives $E(B-V) = 0.07$ mag. These values are in excellent agreement with other estimates of the galactic absorption in the direction of NGC 5061. Burstein & Heiles (1984) found $A_B = 0.25$ from H I/galaxy counts, while Schlegel, Finkbeiner & Davis (1998) deduced $A_B = 0.30$ from the *COBE/DIRBE* and *IRAS/ISSA* maps. In this paper we adopt $A_B = 0.30 \pm 0.05$ as the fiducial value for the total extinction.

4 THE LIGHT CURVES

The *UBVRIJ* light curves of SN 1996X are shown in Fig. 4. We estimated that the SN reached B maximum on 1996, April 18 (JD = 245 0191.5 ± 0.5) at a magnitude $B = 13.24 \pm 0.02$. Following the definition of Phillips (1993), we measured $\Delta m_{15}(B) = 1.31 \pm 0.08$ mag for SN 1996X, in good agreement with previous estimates, i.e. $\Delta m_{15}(B) = 1.28$ (Riess et al. 1998a) and $\Delta m_{15}(B) = 1.25 \pm 0.05$ (Phillips et al. 1999).[1]

The apparent magnitudes in the different bands at the epoch of the respective maxima are listed in Table 5, along with other light-curve parameters. As is normally observed in SN Ia, *V* and *R* maxima occurred 2–3 d later than *B* maximum, while the *U* and *I* maxima preceded it by 4 d.

[1] The correction to $\Delta m_{15}(B)$ caused by the presence of reddening (cf. Section 5) is very small (Phillips et al. 1999) and has been neglected.

Table 2. *UBVRI* photometry for SN 1996X.

Date	Phase* (d)	*U*	*B*	*V*	*R*	*I*	Telescope
14/04/96	−3.7	12.71 ± 0.03	13.29 ± 0.05	13.30 ± 0.02	13.3 ± 0.02	13.42 ± 0.03	ESO/Dutch 0.9m
15/04/96	−2.7	12.75 ± 0.03	13.34 ± 0.02	13.35 ± 0.02	13.26 ± 0.01	13.39 ± 0.03	ESO/Dutch 0.9m
16/04/96	−1.7	12.79 ± 0.02	13.27 ± 0.01	13.29 ± 0.02	13.25 ± 0.01	13.38 ± 0.01	ESO/Dutch 0.9m
16/04/96	−1.6	–	–	13.22 ± 0.01	13.17 ± 0.01	–	ESO 3.6m + EFOSC
17/04/96	−0.8	12.77 ± 0.04	13.25 ± 0.01	13.28 ± 0.01	13.23 ± 0.02	13.43 ± 0.01	ESO/Dutch 0.9m
18/04/96	0.9	–	13.22 ± 0.15	13.30 ± 0.05	13.27 ± 0.02	–	Asiago 1.82m
19/04/96	+1.9	12.94 ± 0.05	13.30 ± 0.01	13.21 ± 0.01	13.18 ± 0.01	13.54 ± 0.02	ESO/Dutch 0.9m
20/04/96	+2.9	13.17 ± 0.09	13.30 ± 0.01	13.22 ± 0.01	13.19 ± 0.01	13.59 ± 0.01	ESO/Dutch 0.9m
23/04/96	+5.9	–	13.51 ± 0.01	13.41 ± 0.01	13.34 ± 0.01	13.81 ± 0.02	ESO/Dutch 0.9m
24/04/96	+7.2	–	13.62 ± 0.01	13.41 ± 0.01	13.43 ± 0.02	13.83 ± 0.02	ESO/Dutch 0.9m
25/04/96	+8.2	–	13.70 ± 0.01	13.45 ± 0.01	13.51 ± 0.01	13.97 ± 0.01	ESO/Dutch 0.9m
26/04/96	+9.2	–	13.79 ± 0.01	13.48 ± 0.01	13.55 ± 0.02	13.98 ± 0.02	ESO/Dutch 0.9m
27/04/96	+10.1	–	13.91 ± 0.01	13.58 ± 0.01	13.60 ± 0.01	14.00 ± 0.01	ESO/Dutch 0.9m
28/04/96	+11.1	–	13.99 ± 0.01	13.67 ± 0.01	13.69 ± 0.01	14.11 ± 0.01	ESO/Dutch 0.9m
04/05/96	+15.9	–	–	–	–	14.11 ± 0.02	ESO 1m + DENIS
05/05/96	+16.9	–	–	–	–	14.11 ± 0.02	ESO 1m + DENIS
05/05/96	+17.0	15.15 ± 0.02	14.83 ± 0.03	14.11 ± 0.02	14.07 ± 0.02	14.16 ± 0.02	ESO/Dutch 0.9m
06/05/96	+17.9	–	–	–	–	14.09 ± 0.01	ESO 1m + DENIS
07/05/96	+18.9	–	–	–	–	14.08 ± 0.01	ESO 1m + DENIS
07/05/96	+19.0	15.37 ± 0.01	15.10 ± 0.01	14.21 ± 0.02	13.96 ± 0.03	14.06 ± 0.02	ESO/Dutch 0.9m
09/05/96	+22.0	15.73 ± 0.02	15.29 ± 0.01	14.23 ± 0.01	14.00 ± 0.02	13.88 ± 0.01	ESO/Dutch 0.9m
10/05/96	+23.0	15.77 ± 0.04	15.50 ± 0.01	14.35 ± 0.01	14.03 ± 0.02	13.73 ± 0.03	ESO/Dutch 0.9m
11/05/96	+24.0	–	–	–	–	14.00 ± 0.01	ESO 1m + DENIS
12/05/96	+25.0	–	–	–	–	13.97 ± 0.01	ESO 1m + DENIS
13/05/96	+26.3	–	–	–	14.14 ± 0.02	13.87 ± 0.03	ESO/Dutch 0.9m
13/05/96	+26.3	16.04 ± 0.01	15.79 ± 0.01	14.53 ± 0.01	14.16 ± 0.02	13.81 ± 0.03	ESO/Dutch 0.9m
14/05/96	+27.2	16.20 ± 0.01	–	14.68 ± 0.01	14.22 ± 0.01	13.97 ± 0.02	ESO/Dutch 0.9m
17/05/96	+29.2	16.26 ± 0.04	16.01 ± 0.01	14.80 ± 0.02	14.44 ± 0.01	14.03 ± 0.03	ESO/Dutch 0.9m
19/05/96	+31.3	16.25 ± 0.16	16.09 ± 0.03	15.01 ± 0.02	14.51 ± 0.01	14.13 ± 0.02	ESO/MPI 2.2m + EFOSC2
22/05/96	+34.2	16.53 ± 0.01	16.22 ± 0.02	15.10 ± 0.02	14.71 ± 0.01	–	ESO/Dutch 0.9m
26/05/96	+39.2	16.75 ± 0.02	16.44 ± 0.01	15.36 ± 0.01	14.95 ± 0.01	14.64 ± 0.01	ESO/Dutch 0.9m
21/06/96	+64.0	–	–	–	15.90 ± 0.04	15.91 ± 0.02	ESO/Dutch 0.9m
24/06/96	+67.1	–	–	16.12 ± 0.01	16.01 ± 0.01	16.10 ± 0.01	ESO/Dutch 0.9m
28/06/96	+72.0	–	16.95 ± 0.01	16.17 ± 0.02	–	–	ESO/Dutch 0.9m
15/07/96	+89.2	–	17.08 ± 0.02	16.67 ± 0.01	16.61 ± 0.01	16.81 ± 0.01	ESO 3.6m + EFOSC
21/07/96	+95.1	17.92 ± 0.01	17.19 ± 0.01	16.77 ± 0.02	16.84 ± 0.01	17.03 ± 0.01	ESO/Dutch 0.9m
06/09/96	+142.1	–	18.10 ± 0.02	–	–	–	ESO/MPI 2.2m + EFOSC2
02/01/97	+259.3	–	19.73 ± 0.06	19.72 ± 0.03	20.40 ± 0.04	–	ESO/Dutch 0.9m
10/02/97	+298.5	–	19.98 ± 0.03	20.28 ± 0.03	–	–	ESO 3.6m + EFOSC
31/03/97	+347.0	–	21.00 ± 0.09	21.06 ± 0.07	21.63 ± 0.12	–	ESO/Dutch 0.9m
5/04/97	+351.6	–	–	21.10 ± 0.08	–	20.86 ± 0.05	HST + WFPC2
5/04/97	+351.6	–	–	21.04 ± 0.05	–	20.78 ± 0.05	HST + WFPC2
18/04/97	+365.0	–	21.36 ± 0.10	21.34 ± 0.09	–	–	ESO/Dutch 0.9m
1/09/97	+501.2	–	23.72 ± 0.13	23.71 ± 0.13	–	–	HST + WFPC2
1/09/97	+501.2	–	23.68 ± 0.20	23.89 ± 0.13	–	–	HST + WFPC2

* Relative to the epoch of *B* maximum JD = 245 0191.5.

Table 3. Infrared photometry for SN 1996X.

Date	Phase* (d)	*J*	*H*	*K′*
29/04/96	+12.3	15.24 ± 0.05	14.19 ± 0.04	14.17 ± 0.06
04/05/96	+16.0	15.05 ± 0.11	–	≤14.0
05/05/96	+16.9	15.02 ± 0.10	–	–
06/05/96	+17.9	14.89 ± 0.10	–	–
07/05/96	+18.9	15.12 ± 0.13	–	–
11/05/96	+24.0	14.67 ± 0.07	–	–
12/05/96	+25.0	14.56 ± 0.07	–	–
23/08/96	+128.0	–	≤17.0	≤15.0

* Relative to the epoch of *B* maximum JD = 245 0191.5.

The I light curve shows the secondary maximum typical of 'normal' SNe Ia. This occurs ∼25 d after *B* maximum at a magnitude of 13.90, i.e. 0.50 mag fainter than the first maximum. At the same epochs a noticeable shoulder appears in the *R* curve, and a weaker one in *V*. The few available *J* observations appear to occur in the brightening phase to secondary maximum.

The light curves of SN 1996X are similar to those of other 'normal' SNe Ia, e.g. SN 1994D or SN 1992A. The decline rate of SN 1996X is the same as that of SN 1994D $\Delta m_{15}(B) = 1.32 \pm 0.05$, and slightly smaller than for SN 1992A, $\Delta m_{15}(B) = 1.47 \pm 0.05$ mag (Phillips et al. 1999).

In Fig. 5 we plot the difference between the photometry of SN 1996X and those of other well studied SNe Ia. The light curves were normalized to the apparent maximum in the given band and to the epoch of *B* maximum, and the differences were computed relative to the phase of SN 1996X observations (the light curves of the other SNe were interpolated when necessary). We selected as a comparison the normal SNe 1992A and 1994D, and also SNe 1991bg ($\Delta m_{15}(B) = 1.93 \pm 0.10$), 1998bu ($\Delta m_{15}(B) = 1.01 \pm 0.05$) and 1991T ($\Delta m_{15}(B) = 0.94 \pm 0.05$) to cover the entire range of SN Ia luminosity evolution.

Some systematic differences are apparent from this figure. In

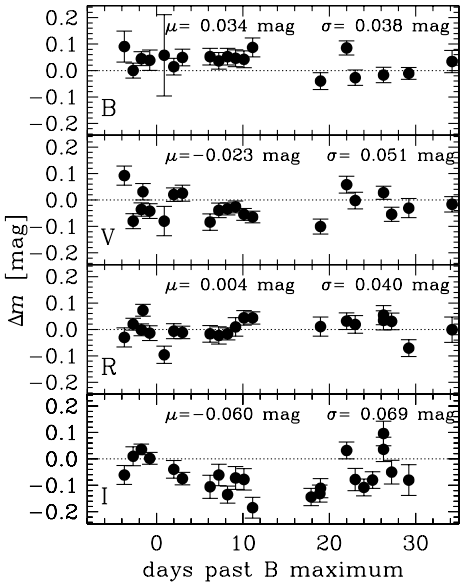

Figure 3. Comparison of the BVRI photometry of SN 1996X presented in this paper with that published by Riess et al. (1999). Also indicated are μ the average difference and σ the rms around the mean.

Table 4. Journal of the spectroscopic observations.

Date	Phase* (d)	Range (Å)	Res. (Å)	Instrument
14/04/96	−3.8	4600–6700	2.5	ESO1.5+B&C+gr10
16/04/96	−1.7	3700–7000	16	ESO3.6+EF+B300, R300
17/04/96	−0.8	4600–6700	2.7	ESO1.5+B&C+gr10
18/04/96	0.2	3100–10700	18	ESO1.5+B&C+gr2
19/04/96	1.2	3100–10700	15	ESO1.5+B&C+gr2
21/04/96	+3.9	4200–8600	30	Asiago1.8+B&C+150tr
25/04/96	+7.2	3100–10500	11	ESO1.5+B&C+gr2
30/04/96	+12.1	4100–6800	14	ESO1.5+B&C+gr5
10/05/96	+22.0	3100–10600	11	ESO1.5+B&C+gr2
12/05/96	+24.3	3100–10600	11	ESO1.5+B&C+gr2
19/05/96	+31.3	3200–9100	11	ESO2.2+EF2+gr6, 5, 1
13/06/96	+56.0	3100–10400	13	ESO1.5+B&C+gr2
14/06/96	+57.1	3100–10400	14	ESO1.5+B&C+gr2
14/07/96	+87.6	3100–10600	15	ESO1.5+B&C+gr2
20/12/96	+246.0	3500–9300	8	ESO1.5+B&C+gr25
10/02/97	+298.4	3700–6900	16	ESO3.6+EF+B300

*Relative to the epoch of B maximum JD = 245 0191.5.

the B-band the difference is greatest at around phase 20 d, and then it remains constant or decreases. This is of course the reason why $\Delta m_{15}(B)$ is so effective in discriminating between SNe Ia light curves. In the V- and R-bands, the picture is less clear. Whereas in the B-band the SNe closest to SN 1996X are SNe 1992A and 1994D, as expected because of the similar $\Delta m_{15}(B)$, in the R-band the best match to SN 1996X is SN 1998bu. This is true also in the I-band. Indeed, in SNe 1996X and 1998bu the I secondary maximum occurred at the same phase, i.e. 4–5 d later than in SN 1994D and was 0.15-mag fainter with respect to the first maximum.

SN 1996X is one of the very few SNe for which observations at epochs larger than 1 yr are available. The importance of the late light curve is that it provides useful insights into the process of radioactive energy deposition. The photometry of SN 1996X at day 500 is particularly accurate because it was obtained with *HST*, the superior angular resolution of which allows a positive target

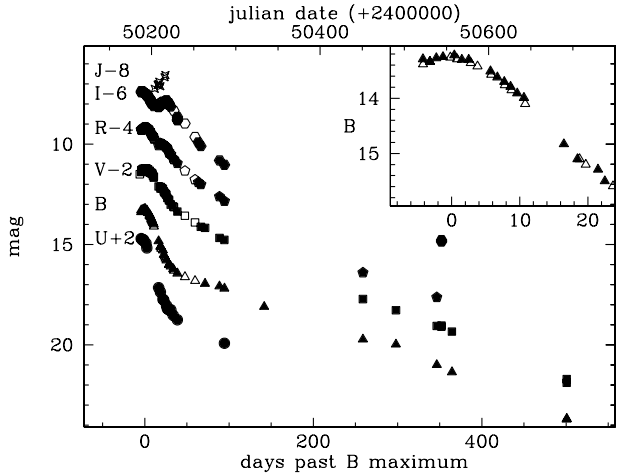

Figure 4. The *UBVRIJ* light curves of SN 1996X; ordinate scale refers to the B-band, other bands are shifted by the amount reported in the legenda. Filled symbols are the values presented in this paper and open symbols are the estimates published by Riess et al. (1999).

identification and a more accurate background subtraction. It is also important that observations were obtained in different bands, giving an estimate of the $B-V$ colour. The result is $B-V_{(500\,\mathrm{d})} = -0.21 \pm 0.24$, which shows that the colour, and thus possibly the spectral shape as well, did not change significantly after day 150.

After day 150, and up to the epoch of the last observation, the light curves are remarkably linear in all bands. The decline rate is 1.7 mag $(100\,\mathrm{d})^{-1}$ in B and V, and slightly smaller (1.4 mag $(100\,\mathrm{d})^{-1}$) in R, although the photometric coverage in this band is not so good.

A comparison between the late V light curves of SN 1996X and those of the SNe Ia 1993L and 1992A (Cappellaro et al. 1997), normalized to the epoch and magnitude of maximum, is shown in Fig. 6. Up to day 400 the three light curves are similar, but later on SN 1996X declines at a much faster rate than the other two objects. The luminosity decline of SNe 1992A and 1993L is very close to the decline of energy release from ^{56}Co decay, which translates to 0.98 mag $(100\,\mathrm{d})^{-1}$. Since at such late phases γ-ray deposition is very small, this pattern may be taken to indicate that complete deposition of positrons is the principal source of power for the light curve. Indeed, Cappellaro et al. (1997) could fit one very late point (1000 d) in the light curve of SN 1992A using a very large positron opacity, thus suggesting complete positron deposition. On the other hand, a normal value $\kappa_{e^+} = 7\,\mathrm{cm^2\,g^{-1}}$ can successfully explain the point at 500 d in the light curve of SN 1996X.

5 THE COLOUR CURVES

With the remarkable exception of the few 'subluminous' SNe Ia, e.g. 1991bg and 1997cn (Turatto et al. 1996, 1998), the colour curves of normal SNe Ia have similar shapes. Indeed, the $B-V$ colour evolution of SN 1996X (Fig. 7) is very similar to those of the 'normal' SNe 1992A and 1994D, and also to that of the bright SN 1991T, the luminosity decline of which was much slower ($\Delta m_{15}B = 0.94$ mag, Phillips 1993).

However, a detailed examination of the early phases shows that even after correction for galactic reddening small shifts remain between the colour curves of different SNe. This may be attributed

Table 5. SN 1996X photometric parameters: the apparent magnitudes and epochs of maximum in the different bands; the colours at the epoch of B maximum; the decline rate Δm_{15}^{B} and Δm_{20}^{V} (Hamuy et al. 1996), and the average decline rate (units are mag $(100\,\mathrm{d})^{-1}$) in three different section of the light curve, namely 5–30 d (β), 50–150 d (γ_1) and >150 d (γ_2).

Maximum	U	B	V	R	I
JD (+245 0000)	188.0 ± 1.0	191.5 ± 0.5	193.5 ± 0.5	194.5 ± 0.5	188.0 ± 1.0
mag	12.73 ± 0.03	13.24 ± 0.02	13.21 ± 0.01	13.19 ± 0.01	13.38 ± 0.01
Δm_{15}		1.31 ± 0.05			
Δm_{20}			1.05 ± 0.05		
β	12.0 ± 0.6	11.4 ± 0.3	6.2 ± 0.1	4.0 ± 0.3	0.21 ± 0.2
γ_1	2.1 ± 0.2	1.60 ± 0.10	2.52 ± 0.09	2.96 ± 0.07	3.7 ± 0.2
γ_2	–	1.71 ± 0.05	1.73 ± 0.05	1.40 ± 0.2	–
Colours†	$U-B$	$B-V$	$V-R$	$V-I$	
	-0.45 ± 0.05	0.00 ± 0.03	0.04 ± 0.02	-0.20 ± 0.05	

† Measured at the epoch of B maximum.

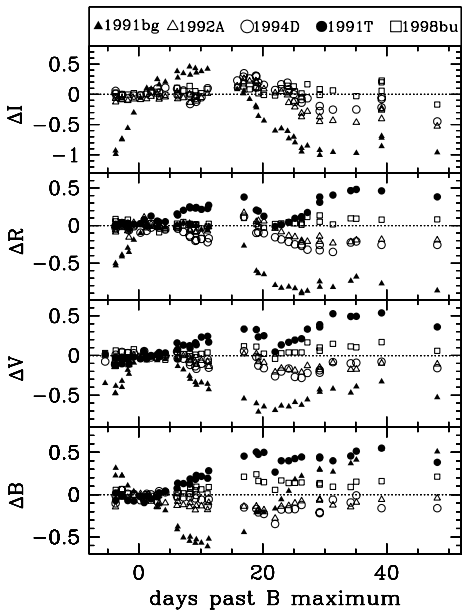

Figure 5. Difference of the light curve of SN 1996X with that of representative SN Ia. For the comparison the light curves were normalized to the magnitude and epoch of maximum.

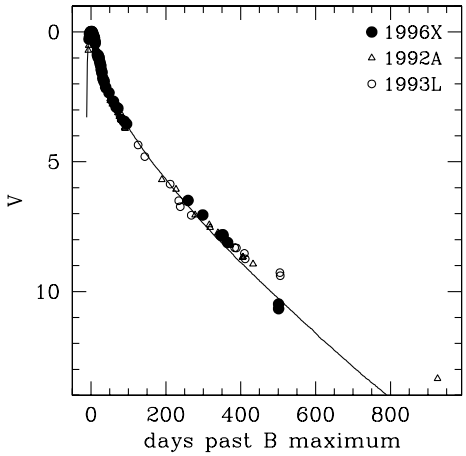

Figure 6. The V late light curve of SN 1996X is compared with that of SN 1993L and 1992A (cf. Cappellaro et al. 1997) and with a W7 light curve model (cf. 7).

to reddening in the host galaxy or to intrinsic differences between the SNe or more likely to both effects. However, the discrepancy between the photometry from different groups shown in Fig. 3 and in Jha et al. (1999) suggests that differences in colour smaller than 0.1 mag should not be overinterpreted. This implies that the comparison of the colour curves cannot yield a reliable estimate of the absorption if this is smaller than $A_B \sim 0.5$ mag. For SN 1996X all we can say is that the colour curve is consistent with negligible reddening in the SN host galaxy.

6 THE ABSOLUTE MAGNITUDE OF SN 1996X

The absolute magnitude of SN 1996X can be derived from the distance of the parent galaxy or conversely we can use the relation between the light-curve shape and the SN absolute magnitude and hence derive the distance.

An estimate of the distance to NGC 5061 can be obtained from the recession velocity and the Hubble law. After correcting the measured heliocentric velocity ($2065 \pm 46\,\mathrm{km\,s^{-1}}$ (da Costa et al. 1998) for the Local Group infall on to Virgo ($1949\,\mathrm{km\,s^{-1}}$) and using $H_0 = 65\,\mathrm{km\,s^{-1}\,Mpc^{-1}}$ we obtain a distance modulus $\mu = 32.38$.

Faber et al. (1989) estimated the distance using the D_n–σ relation. On the same $H_0 = 65\,\mathrm{km\,s^{-1}\,Mpc^{-1}}$ distance scale they obtained a much smaller value, $\mu = 31.32 \pm 0.4$.

Alternatively, we can use the relation between M_B versus Δm_{15} to calibrate the SN absolute magnitude. Depending on the calibration adopted, we obtain $M_B = -19.08 \pm 0.21$ (Hamuy et al. 1996a) or $M_B = -19.48 \pm 0.21$ (Phillips et al. 1999), which corresponds to a distance modulus of $\mu = 32.02 \pm 0.2$ and 32.42 ± 0.2, respectively. The large offset between the two calibrations has been attributed to the use of different recipes for the correction of both galactic and host galaxy extinction (Phillips et al. 1999).

The absolute magnitude of SNe Ia can also be calibrated using the *multicolour light-curve shapes* (MLCS) method (Riess et al. 1996, 1998a). In this approach, the light curve of the SN under study is compared with those of template objects to obtain a simultaneous estimate of the 'luminosity correction' Δ and of the extinction. Although from a statistical point of view this method is

expected to be more robust than the simple $M_B - \Delta m_{15}$ relation, the results are actually very sensitive to the calibration of the template objects, in particular the adopted distance and reddening. This is because the purported monotonic relation between absolute magnitude and colour, with intrinsically brighter SN being bluer, is not yet fully confirmed. This is manifested in the large difference in the template colour curve calibration between Riess et al. (1996) and Riess at al. (1998a).

With reference to SN 1996X, Riess et al. (1998a; fig. 13 therein) showed that the MLCS fit of the V and $B - V$ curves yields $\Delta = +0.25$, $E(B - V) = 0.0$ and a calibrated absolute magnitude $M_B = -19.15$. Therefore, the distance to NGC 5061 is derived to be $\mu = 32.4$ (see also Riess et al. 1998b). This is the same result as obtained from the latest calibration of the $M_B - \Delta m_{15}$ relation (Phillips et al. 1999). However, there is an inconsistency with regard to the total observed reddening, which was estimated to be negligible, whereas the evidence for significant galactic reddening is compelling. (cf. equation 3). Some inconsistencies in the determination of the reddening using the MLCS method were also noticed by Turatto et al. (1998) in the case of SNe 1997cn and 1991bg.

The implication of the difference of the SN absolute magnitude calibration, summarized in Table 6, for the modelling will be addressed in the next sections.

Given that NGC 5061 is an elliptical galaxy, a further independent determination of the distance could be obtained using the globular cluster luminosity function method.

7 THE BOLOMETRIC LIGHT CURVE

Combining *HST* UV data, UBVIR data in the optical and JHK data in the IR for SN 1992A, Suntzeff (1996) computed the so-called *uvoir* bolometric luminosity, which integrates the flux emitted in the range 200–2200 nm, but only up to day 77. In all other cases the bolometric light curve of SN Ia was calculated from data with incomplete wavelength coverage assuming that 'normal SNe Ia' behave similarly. This is the approach we adopt here to derive the *uvoir* bolometric light curve of SN 1996X, since only optical-band observations are available. We integrated the flux emitted in the Johnson–Cousins U, B, V, R, I passbands at the epochs for which measurements are available (for a few epochs the U magnitude was interpolated between points adjacent in time). This was then corrected to the 200–2200 nm adopting the appropriate 'bolometric' correction as given in Suntzeff (1996) for SN 1992A.

As a justification for using this approach we note that the optical spectra and the light curve of SN 1996X are similar to those of SN 1992A. It is also important that at any epoch the UV and infrared emission account for at most 25 per cent of the total flux.

For at least the one epoch when J, H and K photometry for SN 1996X is available we could measure the IR luminosity contribution. We find that on day +12 the infrared luminosity is about 10 per cent of the total *uvoir* luminosity, in very good agreement with the estimates of Suntzeff (1996) for the same epoch. Day 77 is the latest epoch for which Suntzeff gives a 'bolometric correction' for the optical flux. For later epochs a constant optical to bolometric correction was adopted.

The *uvoir* bolometric light curve for the first 100 d, corrected for galactic reddening and for a distance modulus $\mu = 32.02$ is plotted in Fig. 8 (if we adopted $\mu = 32.42$ the bolometric light curve would peak at $\log L = 43.15$). For comparison we also show the *uvoir* bolometric light curve of SN 1994D obtained using the data of Patat et al. (1996) and assuming $\mu = 30.68$ and $A_B = 0.24$.

The observed light curves of SN 1996X were compared with a synthetic light curve obtained with the simple Monte Carlo light curve code used in Cappellaro et al. (1997). The synthetic bolometric light curve was computed for a W7 density structure, with an ejecta mass of $1.38\,M_\odot$ and a synthesized ^{56}Ni mass of $0.6\,M_\odot$. The synthetic light curve reproduces the *uvoir* bolometric light curves of both SNe 1994D and 1996X quite well near maximum. On the other hand, if we adopt the Phillips et al. (1999) calibration ($M_B = -19.48$), the fit of the light-curve peak requires a Ni mass of $0.85\,M_\odot$. This estimate, does not depend much on the particular model of the ejecta, would place SN 1996X near the high-Ni mass end of Chandrasekhar mass models of SNe Ia. If we consider that for its decline rate SN 1996X is expected to be fainter than the average of 'normal' SNe Ia, other SNe would be very difficult to explain within the Chandrasekhar mass explosion scenario.

About 2 weeks past maximum the observed luminosity decline becomes steeper. This is an epoch when the rapidly decreasing

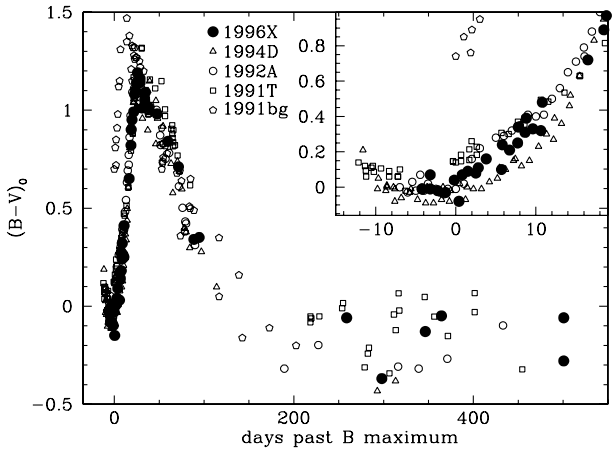

Figure 7. A comparison of the $B - V$ colour curves of SN 1996X and other SNe Ia. In all cases only the galactic reddening (Schlegel et al. 1998) has been removed.

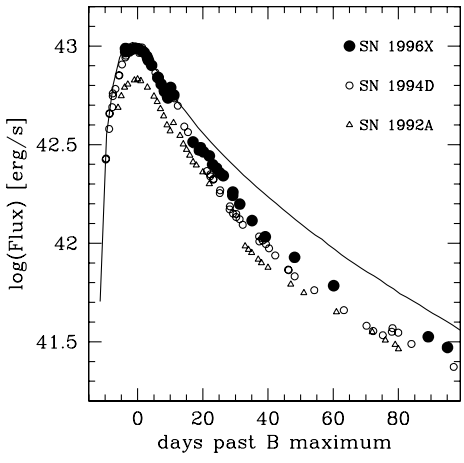

Figure 8. The 'UVOIR' bolometric light curve of SN 1996X ($\mu = 32.02$, $A_B = 0.30$) compared with that of SN 1994D ($\mu = 30.69$, $A_B = 0.24$), SN 1992A ($\mu = 31.35$, $A_B = 0.0$) and with a W7 light-curve model (cf. Section 7).

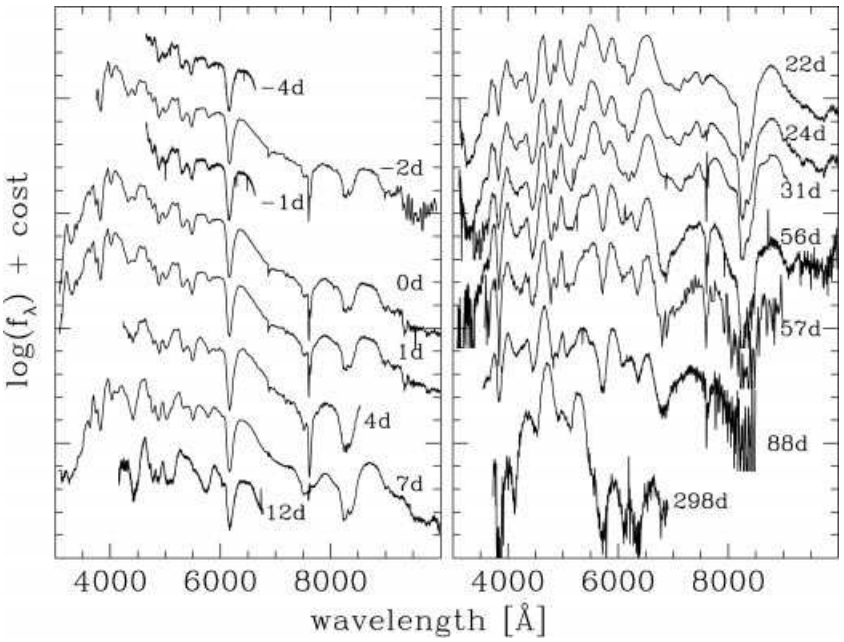

Figure 9. The spectral evolution of SN 1996X. Wavelength scale is in the observer rest frame.

temperature may lead to a decreasing optical opacity. Also, the opacity is probably a function of the elemental abundance in the ejecta, and the combination of these two effects is possibly at the basis of the observed 'Phillips relation' between M_B(max) and $\Delta m_B(15)$. Since the optical opacity was treated as being constant in our code ($\kappa_{\rm opt} = 0.15\,{\rm cm^2\,g^{-1}}$), this behaviour is not reproduced.

At later epochs ($t \geq 300$ d) positron deposition becomes the dominant source of power for the light curve. The synthetic curve was computed using the standard value for the positron opacity, $\kappa_{e^+} = 7\,{\rm cm^2\,g^{-1}}$. As the bolometric correction at these phases is unknown, we compared the model with the V observations, after matching the magnitude at maximum (Fig. 6). This comparison is justified if the bolometric correction is constant which, for epochs >150 d, is supported by the fact that the colour remains constant. It results that the model reproduces the V light curve of SN 1996X between 250 and 500 d rather well, considering the large errors in the photometry at these advanced epochs. Both SNe 1992A and 1993L lie well above the synthetic light curve at $t > 400$ d. As already discussed by Cappellaro et al. (1997), this difference may imply that positron deposition was more efficient in those SNe than in SN 1996X. Whether this requires different explosion models, magnetic field characteristics or degree of ionization is not yet clear (Milne, The & Leising 1999).

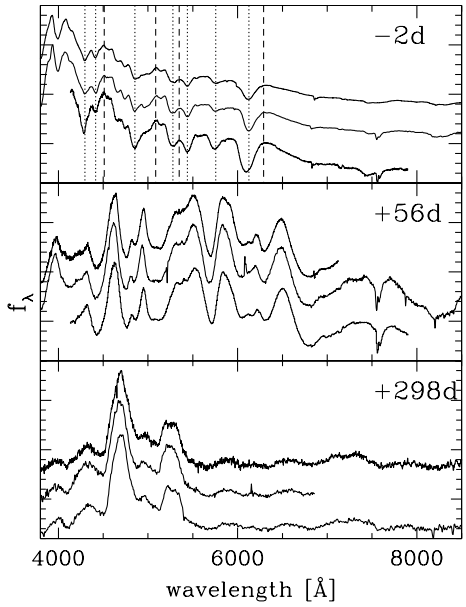

Figure 10. Comparison of spectra of SN 1996X (middle) at different phases with that of SN 1994D (top) and SN 1992A (bottom) at similar phases. Vertical lines in the top panel trace the position of the main absorption and emission features.

8 THE SPECTRAL EVOLUTION

Spectra of SN 1996X have been obtained at 16 epochs, from phase −4 d to +298 d, following the rapid evolution during the early phases in detail and sampling more sparsely the slow late evolution. They are presented in Fig. 9.

The spectral evolution of SN 1996X is similar to that of other normal SNe Ia. At early phases the continuum is very blue and it is dominated by lines attributed to the Fe-group (Fe, Co) and intermediate mass elements (in particular, Si, Ca, S, Mg). The lines exhibit the characteristic P-Cygni profiles with the minima of the absorption components shifting towards longer wavelengths (smaller expansion velocities) with time. At 2–3 months after maximum the continuum is significantly redder ($T_{BB} \sim$ 5–6000 K), and nebular lines of [Fe II] and [Fe III] begin to appear. At about 300 d these are the dominant features in the spectrum.

Exceptionally bright or dim SNe Ia (e.g. SN 1991T and SN 1991bg) can easily be distinguished on the basis of their spectra, but differences also exist among 'normal' SNe Ia. These are more evident before maximum and in the nebular phase, but they disappear in the 2–3 months following maximum (cf. Li et al. 1999). In any case, differences among the spectra of 'normal' SNe Ia are small and can be appreciated only when observations of high signal-to-noise ratio are compared.

Table 6. Estimates of the distance of NGC 5061 and the magnitude of SN 1996X according to various authors.

Source	μ	$M(B)$
D_n–σ Faber et al. (1989)	31.32 ± 0.4	-18.38 ± 0.40
$v_{\text{local group}}$	32.80 ± 0.4	-19.86 ± 0.40
$\Delta m_{15}(B)$ & Hamuy et al. (1996)	32.02 ± 0.2	-19.08 ± 0.21
$\Delta m_{15}(B)$ & Phillips et al. (1999)	32.42 ± 0.2	-19.48 ± 0.21
Riess et al. (1998a,b)	32.4	-19.16

Table 7. The measured position, of the lines of Si II and Ca II, and their expansion velocity.

ph*	Si II (Å)	v_{exp}(Si II) (10^3 km s^{-1})	Ca II (Å)	v_{exp}(Ca II) (10^3 km s^{-1})
−3.8	6158 ± 4	11.4 ± 0.2	–	–
−1.7	6161 ± 8	11.2 ± 0.4	3824 ± 3	11.8 ± 0.2
−0.8	6162 ± 2	11.2 ± 0.1	–	–
+0.2	6165 ± 4	11.0 ± 0.2	3820 ± 4	12.0 ± 0.3
+1.2	6165 ± 4	11.0 ± 0.2	3822 ± 4	11.9 ± 0.3
+3.9	6169 ± 5	10.9 ± 0.2	–	–
+7.2	6167 ± 4	10.9 ± 0.2	3822 ± 4	11.9 ± 0.3
+12.1	6173 ± 4	10.7 ± 0.2	–	–
+22.0	6185 ± 4	10.1 ± 0.2	3826 ± 4	11.6 ± 0.3
+24.3	6190 ± 4	9.9 ± 0.2	3828 ± 4	11.4 ± 0.3
+31.3	6194 ± 5	9.7 ± 0.2	3829 ± 4	11.2 ± 0.4
+56.0	–	–	3840 ± 5	10.6 ± 0.2
+57.1	–	–	3839 ± 9	10.8 ± 0.5
+87.6	–	–	3841 ± 8	10.4 ± 0.3

* Relative to the epoch of B maximum JD = 245 0191.5.

In Fig. 10 we compare the spectra of SN 1996X with those of two SNe with a similar luminosity decline, SN 1992A and SN 1994D. The comparison is made at three different epochs: near maximum, two months and 300 d after maximum. The spectra are *almost* identical. One difference is that near maximum the 6355 Å Si II absorption in SN 1992A is more blueshifted than in both SN 1996X and SN 1994D. This indicates that the average Si II velocity is larger by $\sim$1200 km s^{-1} in SN 1992A. A similar difference in velocity is seen in other Si II lines, e.g. the 5958–5979 Å line, which produces weak absorption near 5800 Å, but not in lines of Si III or S II.

Another difference near maximum is a faint line at 4950 Å, which appears to be stronger, or better resolved, in the spectrum of SN 1996X. This feature is probably due mostly to Fe III lines, and may indicate a higher degree of ionization in SN 1996X compared with the other two SNe.

Finally, the ratio of the deep Fe III absorption at 4250 Å and of the neighbouring weak Si III line near 4400 Å is very different in the three SNe. This may be a temperature effect, since the Si III line requires a much higher ionization/excitation temperature, or an abundance effect, deserving further quantitative investigation.

The line velocities of Si II (6355 Å) and Ca II H&K have been measured from the minima of the P-Cygni absorption features, after correcting the spectra for the heliocentric velocity of the galaxy. These values can be taken to represent approximately the photospheric velocity. The velocities are listed in Table 7 and plotted in Fig. 11. They are similar to those of other normal type SNe Ia at equivalent phases (Barbon et al. 1990; Turatto et al. 1996). Closer inspection (Fig. 10) shows that, whereas near maximum the expansion velocity of SN 1996X is similar to that of SN 1994D, and 10 per cent smaller than that of SN 1992A, the velocity decrease of SN 1996X is slow, so that 2 weeks later the velocities of SN 1996X are comparable to those of SN 1992A.

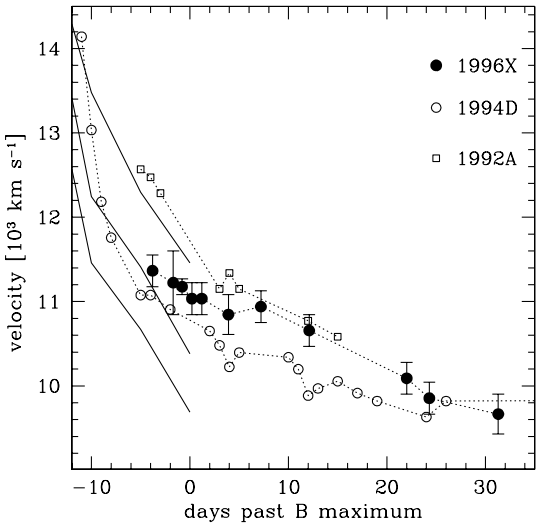

Figure 11. Comparison of the Si II velocities of SN 1996X, SN 1992A, SN 1994D and the model velocities of 10 times normal C + O layer metallicity, normal and 1/10 normal as defined by Lentz et al. (1999) (broken curves, from top to bottom).

Lentz et al. (1999) computed emergent photospheric-phase spectra for a grid of SN Ia atmospheres, and argued that a blueshift of the Si II 6355 Å line could be indicative of an increased metallicity of the SN Ia progenitor. To reproduce the observed range in expansion velocity with the Lentz et al. (1999) models, a change of the metallicity by two order of magnitudes, from 0.1 to 10 times solar, is required. It should be noted that the parent galaxies of the three SNe shown in Fig. 11 are all of early type, either S0 (for SNe 1992A and 1994D) or E (for 1996X), and variations by two orders of magnitude in metallicity between those galaxies are not expected.

The velocity of the Ca II H&K absorption has a different behaviour. It is very similar to the velocity of the same line in SN 1994D, indicating an expansion velocity that is 2000 km s^{-1} slower than for SN 1992A. This supports the conclusions of Wells et al. (1994) that $\Delta m_{15}(B)$ and the Si II velocity do not appear to be correlated, while $\Delta m_{15}(B)$ and the Ca II velocity are. This is not easy to explain since Ca II H&K is a stronger line than Si II 6355 Å and therefore it is even less indicative of the true photospheric expansion velocity.

We have also measured in the near-maximum spectra the R(Si II) and R(Ca II) ratios introduced by Nugent et al. (1995). The values for SN 1996X are 0.25 and 1.39, respectively, very similar to the values typical for 'normal' SNe Ia, in particular SN 1994D, for which the values are 0.29 and 1.38, respectively. According to Nugent et al. (1995), this indicates that the temperature and therefore the Ni mass are similar in these two objects. However, this may be contradicted by the very different strength of the Si III line.

Mazzali et al. (1998) included SN 1996X and other SNe Ia in a diagram showing a correlation between $\Delta m_{15}(B)$ and the FWHM of the 4700 Å nebular feature, which is a blend of [Fe II] and [Fe III] lines, and should thus reflect the mass and distribution of ^{56}Ni. Since the preliminary measurements used by Mazzali et al. (1998) for their plot are confirmed here, that result is also confirmed.

9 SYNTHETIC SPECTRA

We fitted three early-time and one late-time spectra with our various codes in order to gain a deeper understanding of the properties of SN 1996X.

In particular, we modelled the spectra using two different distances. One set of models was computed for $\mu = 32.02$, which is the value obtained from the Hamuy et al. (1996a) calibration of the $M_B - \Delta m_{15}$ relation. This value makes SN 1996X an average SN Ia, comparable to SN 1994D, and somewhat brighter than SN 1992A, even when the larger GCLF distance to this SN is adopted. In fact, SN 1992 has a slightly larger value of Δm_{15} than the other two SNe. Another set of models was computed for the largest distance, $\mu = 32.4$, which was obtained after Phillips et al. (1999). This value makes SN 1996X brighter ($M_B = -19.42$). Different distances imply that different parameters are necessary to produce a synthetic spectrum that fits the observations.

We fitted the early-time spectra using our Monte Carlo code (Mazzali & Lucy 1993), which has been recently improved to include photon branching (Lucy 1999; Mazzali 2000). The code is based on the Schuster–Schwarzschild approximation and uses a large (about 10^6) line data base extracted from the line list of Kurucz & Bell (1995). Radiative equilibrium is assumed in order to compute the temperature structure. The epoch, luminosity and photospheric velocity are input to the code. We used a W7 density structure and mixed composition (Nomoto, Thielemann & Yokoi 1984). For the lower boundary a blackbody radiation field is used. Its characteristic temperature is determined by the temperature iteration, thus taking into account the effect of backwarming resulting from inward travelling energy packets (used to sample the radiation field instead of photons) which are reabsorbed in the photosphere after line absorption and re-emission or electron scattering. Conservation of luminosity above the photosphere ensures a comparison in flux between synthetic and observed spectra.

In order to make our results more sound, we modelled three rather widely spaced epochs: April 18, which is the epoch of B maximum; April 25 and May 10. We adopted $t_B(\max) = 20$ d for the delay of B maximum relative to the epoch of explosion, so our epochs are 20, 27 and 42 d, respectively. When fitting a spectrum with our Monte Carlo code, our input parameters lead to changes in the overall flux (L), in the line velocity ($v_{\rm ph}$) and in the overall nature of the spectrum (the temperature, which results from both L and $v_{\rm ph}$ and on the details of the explosion model used). Therefore, given an observed spectrum, an assumed epoch and distance, we may hope that the allowed range of the parameters L and $v_{\rm ph}$ can be at least narrowed down based on the quality of the fit.

The quality of a synthetic spectrum is judged according to its ability to reproduce the observed spectral features. This is essentially the result of deriving an appropriate temperature structure, and hence the correct runs of ionization and excitation with radius, which is equivalent to velocity in a homologously expanding medium such as the SN ejecta.

Since we tested distance moduli that are different by 0.4 mag, our two sets of models have L that differ by almost a factor of 1.5 in order to reproduce the observed flux level. If this change in L is not accompanied by a simultaneous change in $v_{\rm ph}$, the two sets of models will have temperatures different by a factor of $\sim 1.5^{1/4} \sim 1.1$. This would lead to significant differences in the synthetic spectra. On the other hand, an almost identical temperature can be obtained if the increase in L by a factor 5 is accompanied by an increase in $v_{\rm ph}$ by a factor of $\sim 1.5^{1/2} \sim 1.2$. In this case the temperature of the two models is the same, but the photosphere moves significantly in radius/velocity space, and thus the line features have different redshifts: a larger $v_{\rm ph}$ means bluer lines. This is particularly noticeable for those lines that are reasonably well isolated in wavelength space. A second-order effect is also that for a large $v_{\rm ph}$ the amount of ejecta above the photosphere, with which the energy packets released at the photosphere can interact, is smaller. This leads to reduced backwarming and to a flatter temperature structure. If $v_{\rm ph}$ is very large, a given explosion model may not have sufficient mass above the photosphere to yield the observed line strengths. All of these tests are useful to determine which is the better value of the distance, at least given a particular explosion model. We now briefly discuss the models for the three epochs.

9.1 1996, 18 April, day 20 past explosion

The observed spectrum shows signs of a high temperature through the presence of the Si III line at ~4400 Å, the strength of the Si II 6355 Å line and of the two S II features at 5200 and 5400 Å. For the shorter distance, a good fit to the spectrum can be obtained for the following parameters: $\log L = 43.05$ (erg s^{-1}); $v_{\rm ph} = 8000$ km s^{-1}. Other important parameters and the photometry of the synthetic spectrum are listed in Table 8. The best-fitting model is shown in Fig. 12. When the larger distance is adopted, L increases to 43.24. In order to achieve a reasonable temperature and to produce the correct excitation/ionization regime, $v_{\rm ph}$ must increase to 10 000 km s^{-1}. The synthetic spectrum (Fig. 13, broken curve) has the correct lines, but all of these lines are weaker than in the observed spectrum. Because of the large $v_{\rm ph}$, the absorbing mass is, in fact, smaller than in the model for the shorter distance. Also, more flux escapes in the near-UV (below 3200 Å) because line blanketing is not strong enough. Finally, the velocity of lines such as Si II and S II is larger than in the observed spectrum. This shows that the large distance leads to parameters that are less compatible with the observations. As an instructive example, we also show in Fig. 13 (dotted curve) a synthetic spectrum obtained after multiplying the density by a factor of 1.6: the lines are deeper, but the velocities are still incorrect. Therefore, the shorter distance appears to be favoured.

9.2 1996, 25 April, day 27 past explosion

The next epoch we modelled, day 27, is marked by a cooling of

Table 8. Early-time, short-distance models for SN 1996X.

	Epoch	L	$v_{\rm ph}$	$T_{\rm eff}$	T_{BB}	$\rho(ph)$	$M(ab)$	Synthetic					
Date	(d)	(log erg s^{-1})	(km s^{-1})	(K)	(K)	(g cm^{-3})	($M_\odot$)	W	U	B	V	R	$M_{\rm Bol}$
18/04/96	20	43.05	8000	9500	12000	−13.35	0.70	0.50	12.96	13.30	13.21	12.85	−18.90
25/04/96	27	42.91	6750	8200	9700	−13.54	0.84	0.36	13.70	13.70	13.35	13.11	−18.55
10/05/96	42	42.41	2500	8200	10000	−13.40	1.25	0.41	15.82	15.67	14.38	14.10	−17.30

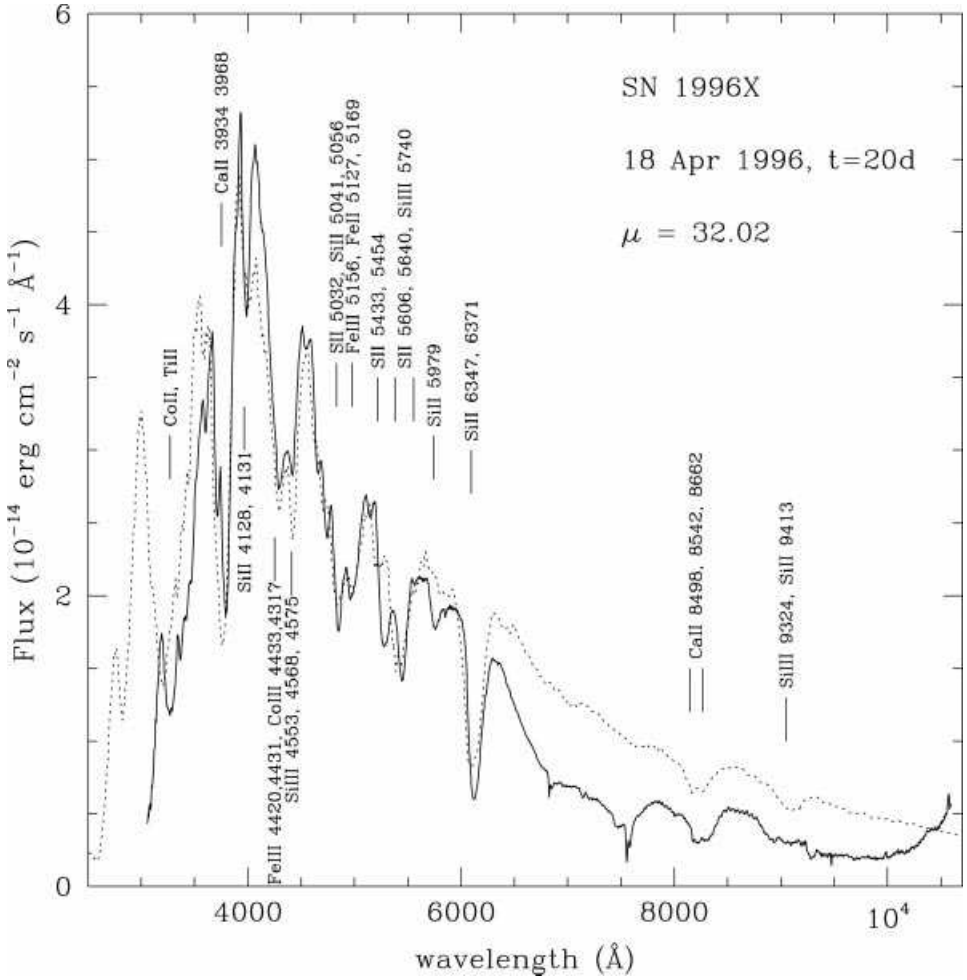

Figure 12. The observed spectrum of SN 1996X on 1996, 18 April, 20-d past explosion (thick curve) is compared with a synthetic spectrum based on W7 computed with the input parameters listed in Table 8 (dotted curve).

the ejecta. This is evident in the disappearance of the Si III line, the strengthening of the Si II and Ca II lines, and the overall redder colour of the spectrum. Our short distance model gives a best fit for $\log L = 42.91$ (erg s^{-1}); $v_{\rm ph} = 6750\,{\rm km\,s^{-1}}$. The temperature (Table 8) is lower than on day 20. The synthetic spectrum is shown in Fig. 14. The poor fit in the red is caused by our assumption of blackbody radiation at the lower boundary. The lack of spectral lines in the red means that the effective opacity is much lower in that region than in the *B* and *V* part of the spectrum, and hence our assumed photospheric radius is larger than its real value. Still, line features (e.g. the Ca II IR triplet) are well reproduced. Elsewhere, the synthetic spectrum fits the observed one well.

9.3 10 May 1996, day 42 past explosion

In the third epoch, the spectrum shows very deep absorptions, indicating that the photosphere has receded deep inside the ejecta. The overall colour is very red ($B - V \sim 1.2$) and all lines are from low-ionization species. Na I D appears as a strong line near 5700 Å. Our best fit for the short distance has $\log L = 42.41$ (erg s^{-1}); $v_{\rm ph} = 2500\,{\rm km\,s^{-1}}$, which is very small. The temperature is also much smaller than at earlier epochs. The synthetic spectrum (Fig. 15) fits the observations reasonably well. The problem with the red flux is now gone, because the photosphere is so deep that the relative change of $R_{\rm ph}$ with λ is small and the low temperature means that the red flux is relatively high. As is typical at these epochs, the Na I D line could only be obtained by adding a small amount of neutral Na (Na I/Na $= 10^{-6}(r)^{-2}$) by hand. We are not aware of any calculation where the Na I D line is correctly reproduced at this advanced epoch [see, for example, the NLTE synthetic spectrum shown in Pauldrach et al. (1996)].

In this case the absolute change of $v_{\rm ph}$ is small, and the overlying mass is large in both cases, so that they cannot be distinguished so easily. Also, the run of ionization with radius is rather flat, because of the low temperature, and thus no line really marks $v_{\rm ph}$, as did, for example, S II at earlier epochs.

At more advanced epochs the spectrum becomes contaminated by nebular emission and cannot be successfully modelled with our Monte Carlo code. Note that the *L*s used at the three epochs are consistent with the values of $L_{\rm Bol}$ derived from the observations in Fig. 8.

9.4 1997, 10 February, day 318

We used a one-zone NLTE code to compute the nebular spectrum at 10 months. The code computes the instantaneous deposition of γ-rays and positrons from the decay of ^{56}Co and uses this as the heat input into the SN nebula, which is bounded by an outer velocity and is composed mostly of Fe at this late epoch. The outer nebular velocity is determined by fitting the width of the

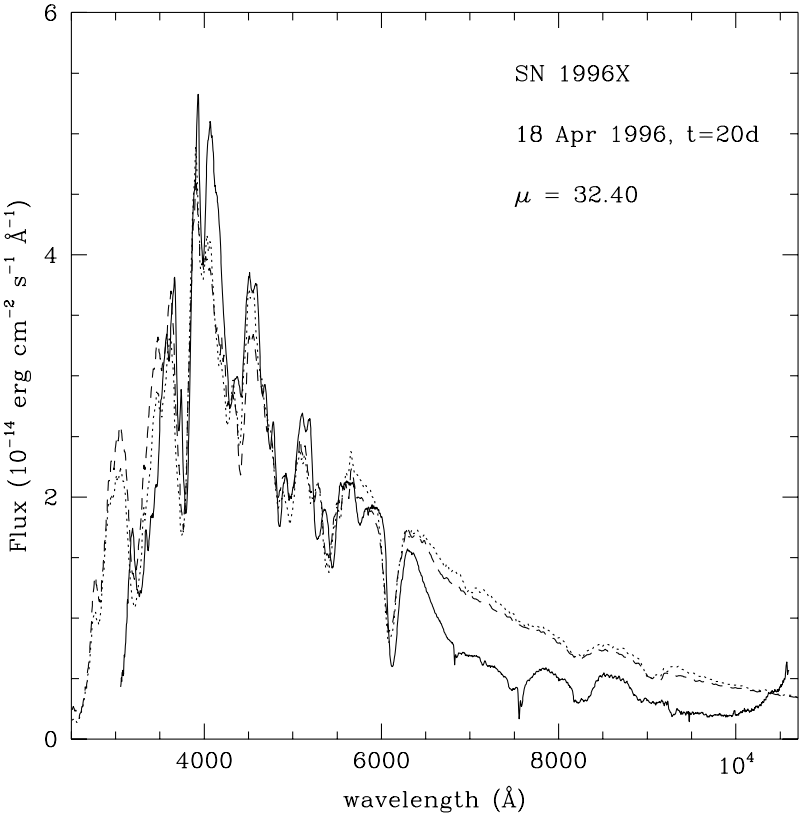

Figure 13. The observed spectrum of SN 1996X on 1996, 18 April (thick curve) is compared with two synthetic spectra obtained for a large distance: the dotted curve is a spectrum computed using W7 with $v_{\rm ph} = 10\,000\,{\rm km\,s^{-1}}$; the broken curve is a spectrum computed with the same parameters but an *ejecta* mass increased by a factor of 1.6.

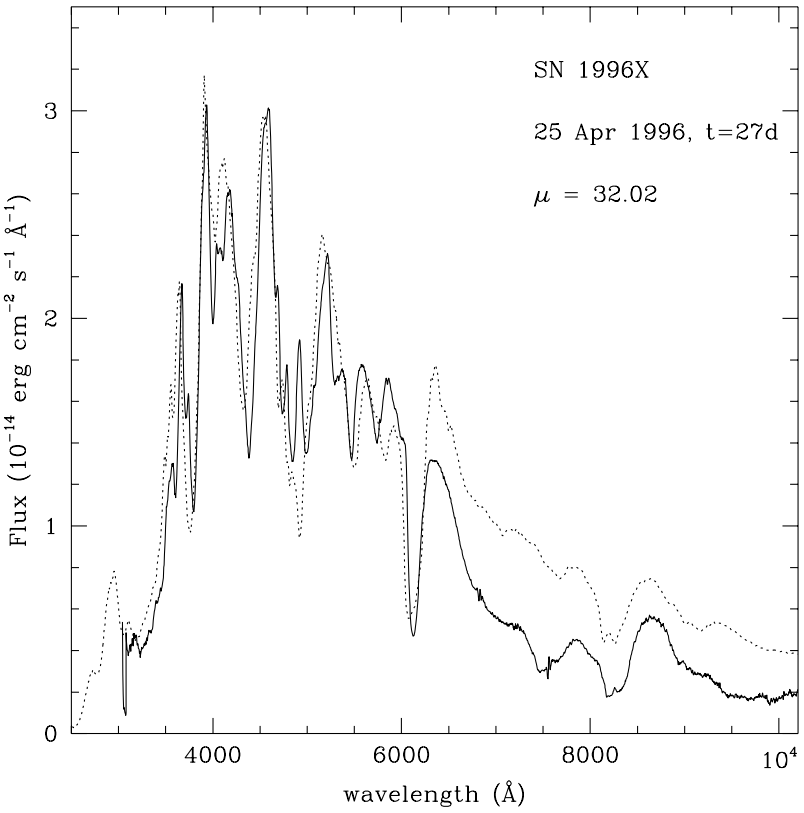

Figure 14. The observed spectrum of SN 1996X on 1996, 25 April (thick curve) is compared with a synthetic spectrum based on W7 computed with the input parameters listed in Table 8 (dotted curve).

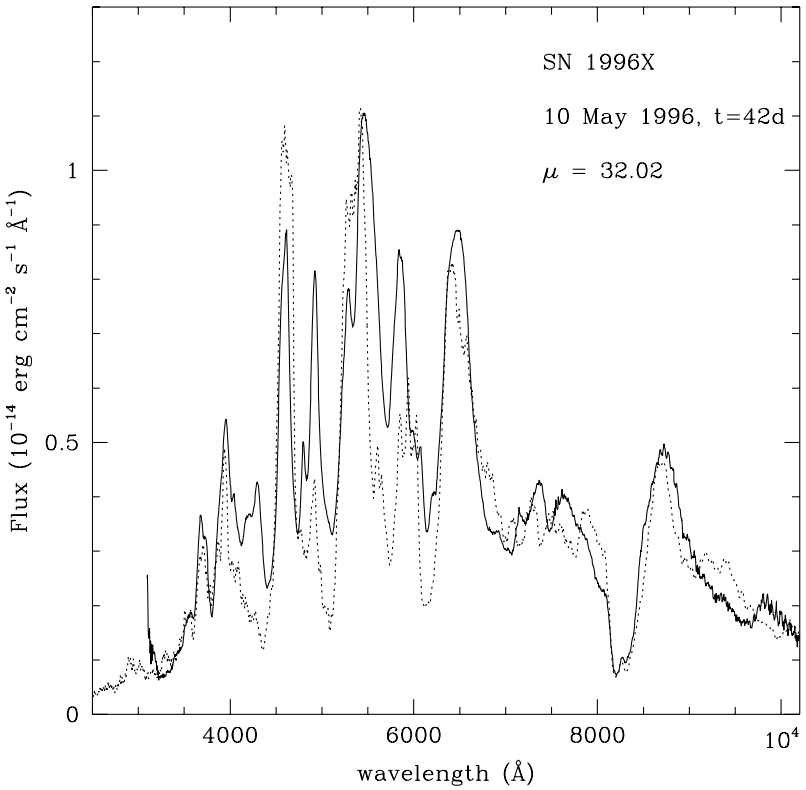

Figure 15. The observed spectrum of SN 1996X on 1996, 10 May (thick curve) is compared with a synthetic spectrum based on W7 computed with the input parameters listed in Table 8 (dotted curve).

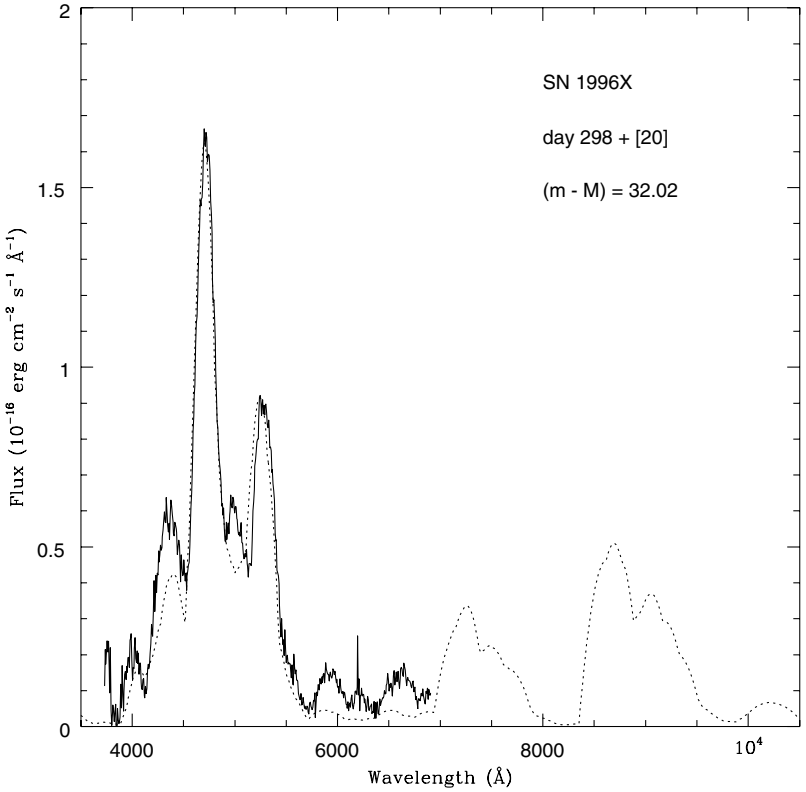

Figure 16. The observed spectrum of SN 1996X on 1997, 10 February (thick curve) is compared with a synthetic NLTE nebular spectrum computed using $M(\mathrm{Ni}) = 0.61\,\mathrm{M}_{\odot}$ and $v = 9250\,\mathrm{km\,s^{-1}}$ (dotted curve).

emission lines; the temperature and density, and hence the mass of ^{56}Ni as originally synthesized, by fitting the ratio of the two strong lines in the blue. The bluer of these lines is, in fact, a blend of mostly [Fe III] lines, while the redder one contains about equal contributions of [Fe II] and [Fe III] lines.

The spectrum can be fitted equally well for both distances if different ^{56}Ni masses are used. The outer velocity is 9250 km s^{-1}. For the short distance a good fit is obtained for $M(\mathrm{Ni}) = 0.65\,\mathrm{M}_\odot$ and a total mass in the nebula (i.e. within the outer velocity) of $0.70\,\mathrm{M}_\odot$. This can be compared with $M(\mathrm{Ni}) = 0.6\,\mathrm{M}_\odot$ and a total mass of $0.85\,\mathrm{M}_\odot$ contained within 9500 km s^{-1} in W7. The fit is shown in Fig. 16. These values indicate that SN 1996X can be regarded as a 'normal' SN Ia.

If, on the other hand, a long distance is used, a good fit requires $M(\mathrm{Ni}) = 0.88\,\mathrm{M}_\odot$ and a total mass in the nebula within 9500 km s^{-1} of $1.00\,\mathrm{M}_\odot$. This values are larger than in W7, and may lead to a total ejected mass larger than the Chandrasekhar limit if a density distribution similar to that of W7 were adopted at velocities larger than the outer nebular velocity. Clearly, the estimate of the distance has consequences on the interpretation of the properties of SN 1996X.

10 CONCLUSIONS

We have presented photometric and spectroscopic data of Supernova 1996X obtained at ESO-La Silla and Asiago.

By examining the *UBVRIJ* light curves, the colour curves and the spectra, we conclude that SN 1996X is a 'normal' SN Ia, i.e. it does not show peculiarities resembling 'overluminous' or 'underluminous' SNe Ia. We measure $\Delta m_{15}(B) = 1.31 \pm 0.08$ mag, similar to the values found for the 'normal' SNe Ia 1992A and 1994D, the most similar to SN 1996X also in their spectroscopic evolution.

Different absolute magnitudes are obtained if one adopts the distance modulus for the host galaxy obtained by Faber et al. (1989) using the D_n–σ relation or that derived from the distance–redshift relation.

The value of the interstellar extinction $A_B = 0.30$ reported by Schlegel et al. (1998) is consistent with the value we find using the relation between the equivalent width of the Na I D line in the spectra and the interstellar extinction. However, both the *multi-colour light-curve shape* and the *snapshot* methods by Riess et al. (1996, 1998a) yield as a result that the absorption is zero. The problem is that the relations between the light-curve shape and colour and the absolute magnitude of a SN Ia are not yet fully reliable, probably because of problems in estimating distance and reddening in the sample used for the calibration. The same problems may explain the discrepancy between different calibration of the $M_B - \Delta m_{B15}$ relation (Hamuy et al. 1996a; Phillips et al. 1999).

We have modelled four spectra at various epochs, using our Monte Carlo code and a one-zone NLTE nebular code, to investigate the problems related to determining the distance. We found that a large distance is difficult to accommodate. If we use the distance obtained from Hamuy et al. (1996a) calibration of the $M_B - \Delta m_{B_{15}}$ relation, $\mu = 32.02$, reasonable synthetic spectra for the photospheric-epoch can be obtained using a standard W7 density structure. The late-time spectra can be fitted using $M(\mathrm{Ni}) = 0.65\,\mathrm{M}_\odot$, which is appropriate for W7, and a similar value is also necessary to reproduce the light curve near maximum with a Monte Carlo code. However, if we use a larger distance, $\mu = 32.4$, the early time spectra are better reproduced for a photospheric velocity larger than the observed one, the late-time spectra require a larger ^{56}Ni mass, and models in general models favour an ejecta mass larger than the Chandrasekhar mass. For the shorter D_N–σ distance, the opposite problem arises.

One of the main problems in our understanding the properties of SN Ia is that we do not know enough yet about the progenitors and the explosion mechanism of SN Ia. Objects with similar $\Delta m_{15}(B)$ and general spectral behaviour could have different evolution and intrinsic characteristics, in particular different expansion velocities, as shown in Fig. 11, and perhaps also different absolute magnitudes.

We need to obtain more high-quality data for nearby SN Ia and their host galaxies to clarify this, as SN Ia are now the most reliable distance indicators on a cosmological scale, and the value of their absolute magnitude has to be calibrated using nearby objects.

Since the host galaxy of SN 1996X is an elliptical galaxy, the globular cluster luminosity function method (Drenkahn & Richtler 1999; Della Valle et al. 1998) could provide a velocity-independent estimate of its distance.

ACKNOWLEDGMENTS

We thank all the astronomers who kindly observed SN 1996X for us at ESO-La Silla: L. Chevallier, C. Tappert, A.D.F. Metanomski, G. Massone, L.A. Wickmann, I. Van Bemmel, J. Spyromilio, C. Zanin. We especially thank P. Fouque, who provided reduced IJK data of the SN obtained at the DENIS 1-m telescope. This paper was based on observations collected at ESO-La Silla.

REFERENCES

Barbon R., Benetti S., Cappellaro E., Rosino L., Turatto M., 1990, A&A, 237, 79

Bowers E. J. C., Meikle W. P. S., Geballe T. R., Walton N. A., Pinto P. A., Dhillon W. S., Howell S. B., Harrop-Allin M. K., 1997, MNRAS, 260, 663

Burstein D., Heiles C., 1984, ApJS, 54, 33

Cappellaro E., Mazzali ., Benetti S., Danziger I. J., Turatto M., Della Valle M., Patat F., 1997, A&A, 328, 203

da Costa L. N. et al., 1998, AJ, 116, 1

Della Valle M., Kissler-Patig M., Danziger J., Storm J., 1998, MNRAS, 299, 267

Drenkhahn G., Richtler T., 1999, A&A, 349, 877

Faber S. M., Wegner G., Burstein D., Davies R. L., Dressler A., Lynden-Bell D., Terlevich R. J., 1989, ApJS, 69, 763

Hamuy M., Walker A. R., Suntzeff N. B., Gigoux P., Heathcote S. R., Phillips M. M., 1992, PASP, 104, 533

Hamuy M., Suntzeff N. B., Heathcote S. R., Walker A. R., Gigoux P., Phillips M. M., 1994, PASP, 106, 566

Hamuy M., Phillips M. M., Schommer R., Suntzeff N. B., Maza J., Avilés R., 1996a, AJ, 112, 2391

Hamuy M., Phillips M. M., Suntzeff N. B., Schommer R., Maza J., Avilés R., 1996b, AJ, 112, 2398

Hamuy M., Phillips M. M., Suntzeff N. B., Schommer R., Maza J., Smith C., Lira P., Avilés R., 1996c, AJ, 112, 2438

Holtzman J. A., Burrows J. C., Casertano S., Hester J. J., Trauger J. T., Watson A. M., Worthey G., 1995, PASP, 107, 1065

Jha S. et al., 1999, ApJS, 125, 73

Kurucz R. L., Bell B., 1995, Kurucz CD-ROM No. 23,

Landolt A. U., 1992, AJ, 104, 340

Lentz E. J., Baron E., Branch D., Hauschildt P. H., Nugent P. E., 2000, ApJ, 530, 966

Li W. D., Qiu Y. L., Zhu X. H., Hu J. Y., Richmond M. W., Filippenko A. V., Treffers R. R., Peng C. Y., Leonard D. C., 1999, AJ, 117, 2709
Lidman C., Gredel R., Moneti A., 1997, IRAC2b User Manual, ESO
Lucy L. B., 1999, A&A, 345, 211
Madore B. F. et al., 1999, ApJ, 515, 29
Mazzali P. A., Lucy L. B., 1993, A&A, 279, 447
Mazzali P. A., Cappellaro E., Danziger I. J., Turatto M., Benetti S., 1998, ApJ, 499, L49
Mazzali P. A., 2000, A&A, in press
Milne P. A., The L.-S., Leising M. D., 1999, ApJS, 124, 503
Munari U., Zwitter T., 1997, A&A, 318, 269
Nomoto K., Thielemann F.-K., Yokoi K., 1984, ApJ, 286, 644
Nugent P., Phillips M., Baron E., Branch D., Hauschildt P., 1995, ApJ, 455, L147
Patat F., Benetti S., Cappellaro E., Danziger I. J., Della Valle M., Mazzali P. A., Turatto M., 1996, MNRAS, 278, 111
Pauldrach A. W. A., Duschinger M., Mazzali P. A., Puls J., Lennon M., Miller D. L., 1996, A&A, 312, 525
Perlmutter S. et al., 1999, ApJ, 517, 565
Phillips M. M., 1993, ApJ, 413, L105
Phillips M. M., Lira P., Suntzeff N. B., Schommer R. A., Hamuy M., Maza J., 1999, AJ, 118, 1766
Pskovskii IU.P., 1967, Sov. Astron., 11, 570
Pskovskii IU.P., 1977, Sov. Astron., 21, 675
Riess A. G., Press W. H., Kirshner R. P., 1996, ApJ, 473, 88
Riess A. G., Filippenko A. V., Challis P. et al., 1998a, AJ, 116, 1009
Riess A. G., Nugent P., Filippenko A. V., Kirshner R. P., Perlmutter S., 1998b, ApJ, 504, 935
Riess A. G. et al., 1999, AJ, 117, 707
Sandage A., Saha A., Tammann G. A., Labhardt L., Panagia N., Macchetto F. D., 1996, ApJ, 460, L15
Schlegel D. J., Finkbeiner D. P., Davis M., 1998, ApJ, 500, 525
Schmidt B. P. et al., 1998, ApJ, 507, 46
Suntzeff N. B., 1996, in McCray R., Wang Z., eds, IAU Colloq. 145, Supernovae and Supernova Remnants. Cambridge Univ. Press, Cambridge, p. 41
Suntzeff N. B. et al., 1999, AJ, 117, 1175
Suntzeff N. B., 2000, in Holt S. S., Zhang W. W., eds, Cosmic Explosions! The Proceedings of the Tenth Maryland Conference on Astrophysics, Am. Inst. Phys., New York, in press (astro-ph/0001248)
Turatto M., Cappellaro E., Benetti S., Danziger I. J., 1993, MNRAS, 265, 471
Turatto M., Benetti S., Cappellaro E., Danziger I. J., Della Valle M., Gouiffes C., Mazzali P. A., Patat F., 1996, MNRAS, 283, 1
Turatto M., Piemonte A., Benetti S., Cappellaro E., Danziger I. J., Mazzali P. A., Patat F., 1998, AJ, 116, 2431
Umeda H., Nomoto K. I., Kobayashi C., Hachisu I., Kato M., 1999, ApJ, 522, L43
Wang L., Wheeler J. C., Höflich P., 1997, ApJ, 476, L27
Wells L. A. et al., 1994, AJ, 108, 2233

This paper has been typeset from a TEX/LATEX file prepared by the author.